Universal free-energy landscape produces efficient and reversible electron bifurcation

J. L. Yuly[a], P. Zhang[b,1], C. E. Lubner[c], J. W. Peters[d], and D. N. Beratan[a,b,e,1]

[a]Department of Physics, Duke University, Durham, NC 27708; [b]Department of Chemistry, Duke University, Durham, NC 27708; [c]Biosciences Center, National Renewable Energy Laboratory, Golden, CO 80401; [d]Institute of Biological Chemistry, Washington State University, Pullman, WA 99163; and [e]Department of Biochemistry, Duke University, Durham, NC 27710

Edited by Harry B. Gray, California Institute of Technology, Pasadena, CA, and approved July 9, 2020 (received for review May 27, 2020)

For decades, it was unknown how electron-bifurcating systems in nature prevented energy-wasting short-circuiting reactions that have large driving forces, so synthetic electron-bifurcating molecular machines could not be designed and built. The underpinning free-energy landscapes for electron bifurcation were also enigmatic. We predict that a simple and universal free-energy landscape enables electron bifurcation, and we show that it enables high-efficiency bifurcation with limited short-circuiting (the EB scheme). The landscape relies on steep free-energy slopes in the two redox branches to insulate against short-circuiting using an electron occupancy blockade effect, without relying on nuanced changes in the microscopic rate constants for the short-circuiting reactions. The EB scheme thus unifies a body of observations on biological catalysis and energy conversion, and the scheme provides a blueprint to guide future campaigns to establish synthetic electron bifurcation machines.

electron bifurcation | electron transfer | short-circuiting | bioenergetics | chemiosmotic hypothesis

Living systems depend crucially on the efficient interconversion of energy at the molecular scale. Electron bifurcation was recognized by Mitchell as being a key element of the Q cycle in mitochondria (1), but it now describes a broader class of chemical reactions—presently found only in biology—that oxidize a two-electron donor and reduce two spatially separated one-electron acceptors (2–5). One of the electron transfer reactions from the bifurcating species can proceed thermodynamically "uphill" with respect to the two-electron (midpoint) reduction potential of the electron-bifurcating donor, provided that the other electron proceeds sufficiently downhill for the reaction to be spontaneous overall. Thus, electron bifurcation, or its reverse reaction known as electron confurcation, can occur spontaneously. The near free-energy conserving nature of electron bifurcation is the source of its efficiency and novelty; this coupling of "downhill" and uphill electron transfers is astonishingly useful. For example, electron bifurcation is used in the Q cycle of respiration (6) and photosynthesis (7), and to generate low-potential equivalents for CO_2 reduction in methanogenesis (8, 9), nitrogen fixation by nitrogenase (10), hydrogen production by hydrogenases (11), and more (4, 12–16). This use of electron bifurcation by nature to achieve difficult chemical transformations highlights its fundamental place in the toolbox of biological energy transduction (2, 5, 17), and makes electron bifurcation an attractive candidate for biomimetic energy schemes that require the production of highly reducing or oxidizing species (3, 5, 18).

Short-Circuiting Limits Electron Bifurcation Efficiency

The process of electron bifurcation is illustrated in Fig. 1*A*. First, a two-electron donor (D), with a mean reduction potential in the middle of the physiological window, donates its electrons to the electron-bifurcating enzyme. The electrons reach the electron-bifurcating cofactor (B), which sends one electron into a low-potential hopping pathway and one into a high-potential hopping pathway (cofactor chains L and H, respectively). These paths each terminate at electron-accepting substrates, one at high- (A_H) and the other at low- (A_L) reduction potential. In the reverse (confurcating) reaction, one electron flows from A_H and another electron from A_L to doubly reduce the bifurcating species B, which then performs a two-electron reduction of D. For efficient electron bifurcation to occur, one electron must proceed through the low-potential branch for every electron that flows through the high-potential branch. Efficient electron confurcation requires that every electron flowing from the high-potential substrate A_H to species B must be matched with an electron from the low-potential substrate A_L to reduce B. In most electron-bifurcating systems, B is either a quinone or a flavin (4), although transition-metal complexes were proposed to bifurcate electrons (19). The L and H cofactors typically include hemes, iron–sulfur clusters, and/or nonbifurcating quinones and flavins (4, 19).

Nature's electron bifurcation machinery has proven difficult to imitate, and no synthetic molecular machine has been built that carries out high-efficiency electron bifurcation. The obstacle to realizing efficient electron bifurcation arises from the short-circuiting reactions intrinsic to the bifurcating network, indicated in Fig. 1*C* (5, 20, 21). Short-circuit electron transfer reactions occur when an electron flows from the B^- intermediate to the high-potential acceptor A_H, or when electrons individually flow from the low-potential (high-energy) branch to reduce B^-. In addition, direct tunneling from L_1 to H_1 is possible, although the tunneling distance is very large in known electron-bifurcating

Significance

Electron bifurcation is an efficient and reversible redox reaction at the heart of key bioenergetic and biocatalytic reaction pathways used in nature. Electron bifurcation oxidizes a two-electron donor, using the electrons to reduce cofactors on two separate electron-transfer redox chains. The coupling of these redox reactions allows one of the electrons to move thermodynamically uphill, leveraging the downhill flow of the other electron. Thus, electron bifurcation may generate strong oxidants or reductants with minimal free-energy loss (i.e., reversibly). Not surprisingly, life harnesses electron bifurcation in biochemical pathways that perform challenging chemical reactions, including proton translocation across membranes, nitrogen fixation, and CO_2 reduction. We predict that there is one universal free-energy landscape that supports efficient electron bifurcation reactions.

Author contributions: J.L.Y., P.Z., J.W.P., and D.N.B. designed research; J.L.Y. and P.Z. performed research; J.L.Y. contributed new reagents/analytic tools; J.L.Y., P.Z., and D.N.B. analyzed data; and J.L.Y., P.Z., C.E.L., J.W.P., and D.N.B. wrote the paper.

This article is a PNAS Direct Submission.

[1]To whom correspondence may be addressed. Email: peng.zhang@duke.edu or david.beratan@duke.edu.

This article contains supporting information online at https://www.pnas.org/lookup/suppl/doi:10.1073/pnas.2010815117/-/DCSupplemental.

First published August 14, 2020.

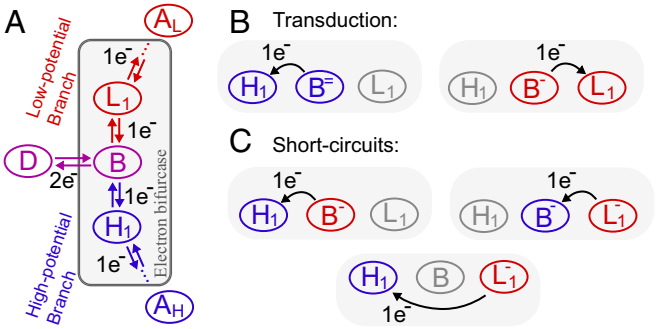

Fig. 1. Electron bifurcation and short-circuit pathways. (*A*) The kinetic network underpinning an electron bifurcation enzyme, and the redox reactions that may take place at the bifurcating site B. There may be additional cofactors in either chain (for instance L_3 or H_4, not explicitly shown). Red indicates the low redox potential (high-energy) path, while blue indicates the high-potential (low-energy) path. Purple indicates the two-electron bifurcating species B, and the two-electron source/sink D. Electron transfer from the electron bifurcation site can result in energy transduction (*B*), but energy-wasting short-circuit reactions (*C*) also occur between the same cofactors.

enzymes (~20 Å or more) (21, 22), substantially slowing this short-circuit reaction.

The Q cycle was the first electron-bifurcation reaction that was found to be reversible on relevant physiological timescales (20). Since the tunneling distances for short-circuit transfers (Fig. 1*C*) are the same as for productive transfers, the rate constants for the productive electron transfers are expected to be similar to those for the short-circuit electron transfers (21). To prevent short-circuiting, "gating mechanisms" were proposed to suppress short-circuiting reactions, including concerted two-electron transfer (21), conformational gating (5, 23), "spring loading" of the Rieske iron–sulfur protein (24), Coulombic interactions (25), and other possible mechanisms termed double-redox gating (20, 21). However, after almost 20 years of searching, no experimental "smoking gun" in support of these gating mechanisms has been found. For example, it is understood that conformational motion of the Rieske iron–sulfur protein is required to explain how electrons tunnel through the high-potential branch. But, this conformational motion does not itself serve as a gating mechanism (to suppress short-circuiting electron transfer rate constants) because the reactions operate under near-reversible conditions (5, 6, 21). Indeed, there is no consensus on how the Q cycle accomplishes reversible operation with such high efficiency.

In addition to the quinone-based Q-cycle complexes, other novel flavin-based electron-bifurcating enzymes were discovered in the last decade (4, 5, 9, 26, 27). Many (if not all) of these flavin-based electron-bifurcating enzymes are also reversible (4), and many are not membrane bound (19, 22); others seem to lack significant conformational flexibility (3, 5, 19). Short-circuiting electron transfer also creates a challenge to flavin-based electron-bifurcating enzymes (5), and how these bifurcating flavoenzymes avoid short-circuiting, while maintaining reversibility, is unknown.

A Thermodynamic Landscape to Enable Efficient Electron Bifurcation

The analysis presented here indicates that a universal mechanism of high-efficiency bifurcation is used by all electron-bifurcating enzymes. We find that the secret to avoiding slippage (short-circuiting electron transfer) in electron-bifurcation reactions lies in the steep free-energy (reduction potential) landscapes of the spatially separated high- and low-potential branches, which is considered to be an enigmatic (but conserved) feature of electron-bifurcating enzymes (4, 5, 28). This landscape has a form similar to the redox potential landscapes in photosynthesis (29), although the mechanism for electron bifurcation is drastically different from that of photosynthesis.

In nature, steep free-energy landscapes are not unique to electron bifurcation. Photosynthesis uses steep landscapes to prevent charge recombination and to induce high-yield electron transfer following photoexcitation (29). Fig. 2 shows nine possible free-energy landscapes for electron bifurcation, discussed in detail below. Only one landscape, indicated in Fig. 2*G* supports efficient electron bifurcation by suppressing short-circuiting (*vide*

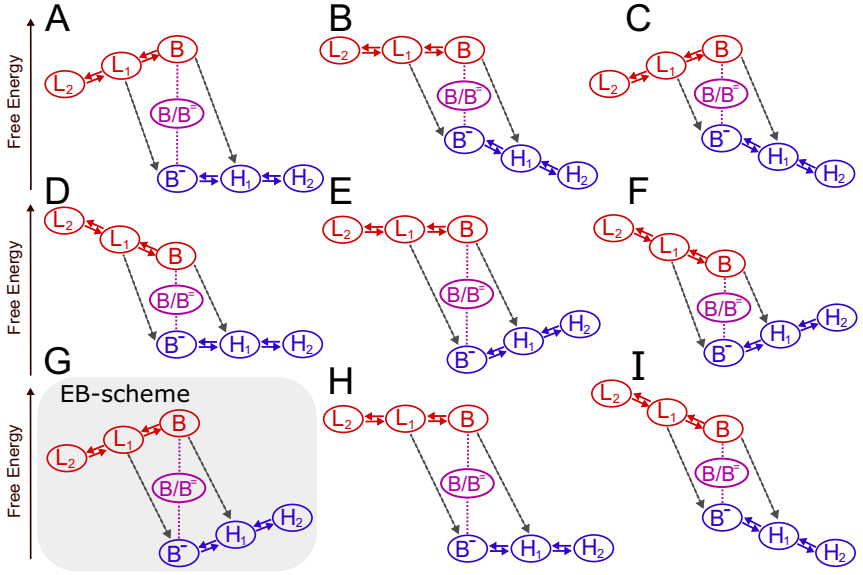

Fig. 2. Candidate free-energy (reduction potential) landscapes for energy-conserving electron bifurcation. Solid arrows represent productive electron transfer steps, and gray dashed arrows represent short-circuit energy-dissipating steps. The purple ovals represent the positions of the two-electron (midpoint) reduction potential of the bifurcating species. Landscapes *A–F* are not free-energy conserving (i.e., they produce irreversible electron bifurcation or confurcation) and therefore are not energetically efficient, while landscapes *H* and *I* produce short-circuiting (Fig. 3). Only landscape *G* is reversible and avoids short circuits, thanks to the Boltzmann suppression of microstates in which short-circuiting can occur.

infra). Without the EB-scheme design principle, successful synthetic electron bifurcation (i.e., the equal and reversible yield of the high- and low-potential redox products) seems tremendously difficult to accomplish. This free-energy design principle, described and analyzed in detail below, explains how nature elegantly skirts a major obstacle (short-circuiting reactions) to producing high-value redox species.

Candidate Free-Energy Landscapes for Electron Bifurcation

There are three main ways that the thermodynamic landscape may influence electron transfer rates in an oxidoreductase. First, electron transfer rate constants in proteins are determined by tunneling pathways and distances between cofactors, reorganization energies, and thermodynamic driving forces (30). Thus, the reduction potential landscapes of the electron bifurcation branches, the cofactor placement, and the protein structure (31) determine the productive and short-circuit electron transfer rate constants. Second, the thermodynamic landscape establishes steady-state populations for each possible redox state. Indeed, these steady-state populations determine the effective activation free energies for short-circuiting electron transfer (*vide infra*). Third, the free-energy difference between initial and final catalytic states determines the catalytic driving force (and hence whether the reaction runs in the forward or reverse direction). The overall driving force for electron bifurcation is

$$\Delta G_{bifur} = 2FE_D - FE_{A_L} - FE_{A_H}, \qquad [1]$$

where E_D, E_{A_L}, and E_{A_H} are the (midpoint) reduction potentials of the D, A_L, and A_H substrates, respectively, and F is Faraday's constant. For electron bifurcation to be spontaneous, $\Delta G_{bifur} < 0$.

Nine possible free-energy landscapes for electron bifurcation are categorized in Fig. 2. Landscapes A, B, and C have $\Delta G_{bifurc} \ll 0$ and hence are not reversible, only operating in the electron bifurcation direction. Landscapes D, E, and F have $\Delta G_{bifurc} \gg 0$ and only operate in the electron confurcating direction. Thus, only landscapes G, H, and I, with $\Delta G_{bifurc} \approx 0$, are suited for reversible electron bifurcation/confurcation. To drive catalysis in the electron bifurcation (confurcating) direction with these landscapes, one would simply tune the reduction potentials of the terminal substrates to tilt the free-energy balance slightly (Eq. **1**) (via reactant concentrations or the transmembrane potential for membrane-bound proteins). The reversibility of electron bifurcation is the source of its energetic efficiency (3, 5, 32).

The EB Scheme

Now, we describe how the EB scheme shown in Fig. 2*G* insulates the kinetic network from short circuits, while producing high-efficiency (reversible) electron bifurcation, and we prove this claim numerically in the next section (the other two energy-conserving landscapes, illustrated in Fig. 2 *H* and *I*, lead to copious short-circuiting and are not viable). The slopes of the H and L redox branches in Fig. 2*G* cause electrons to pile up near B in the low-energy branch (blue), and holes in the high-energy branch (red) near B. Since the one-electron cofactors cannot accept a second electron at relevant potentials and must be in the reduced state to donate an electron, the EB scheme insulates the enzyme against short-circuiting by an electron occupancy blockade effect, despite having large short-circuiting rate constants. For an energy-wasting short-circuiting reaction to occur, a hole must occupy the low-energy branch (blue) and an electron must occupy the high-energy branch. Taken together, these processes create a very large free-energy barrier for short-circuiting. That is, the EB scheme is protected against short circuits by Boltzmann occupancy factors, so the enzyme will rarely enter a state where short circuits can occur. For productive electron bifurcation (confurcation) to occur, only a hole (electron) must move down (up) the low- (high-) energy branch, so the productive transfers have a much smaller free energy of activation to overcome. This occupancy effect, arising from the EB-scheme landscape, can lead to highly efficient partitioning of electrons into the high- and low-potential branches. The viable EB scheme (Fig. 2*G*), examined in detail here, uses crossed potentials at the bifurcating site B, but we have not examined whether crossed potentials are a requirement for effective electron bifurcation; the role of crossed potentials in electron bifurcation was discussed recently (3, 5, 12, 32). Next, we show how these principles emerge quantitatively from a kinetic model for electron bifurcation that describes the electron flux, notably including cofactor occupancy effects.

Many-State, Many-Electron Kinetics of Electron Bifurcation

Attempts were made in earlier studies to model the kinetics of electron bifurcation, and those studies succeed in describing many features of the kinetics. However, some of the previous models are not reversible (3, 21) and, as such, are inconsistent with the known reversibility of biological electron bifurcation. Other models restrict the number of tunneling electrons in the enzyme to just two (33) (inconsistent with access to pools of one- and two-electron redox substrates) or use rate constants that are physically unmotivated (34, 35), including ad hoc turning off of short-circuit reactions (36, 37). The scheme described here avoids these unnatural constraints and treats productive electron transfers (Fig. 1*B*) on the same footing as short circuits (Fig. 1*C*), allowing electrons to tunnel freely with rate constants estimated using nonadiabatic electron transfer theories with appropriate Marcus factors (30, 38), but only when a mobile electron resides on the donor, and a hole on the acceptor (i.e., we explicitly track the occupancies of all redox-active species). The substrates $D^=$, A_H, and A_L were modeled as electron reservoirs, which release and accept electrons at the reduction potential of the substrate, with adjustable rate constants that were tuned so that they are not rate limiting (that is, the intrinsic kinetics of the electron bifurcation enzyme are assumed rate limiting). Two electrons move together in one kinetic step into B. For the Q cycle, this describes quinone diffusion into the Q_0 site. Details of the kinetics model appear in *SI Appendix*.

For each of the three free-energy conserving schemes (Fig. 2 *G–I*) for electron bifurcation, we implemented a minimalistic kinetic model, *mutatis mutandis*, for electron bifurcation enzymes. The model (Fig. 3*A*), and the resulting kinetics at steady state (Fig. 3 *B–F*), are shown in Fig. 3. The B/B^- and $B^-/B^=$ standard reduction potentials were set to −400 and 400 mV, respectively, and the nearest-neighbor distance between cofactors was set to 10 Å (next-to-nearest distance of 20 Å, etc.). Nature's electron bifurcation systems vary these parameters, but the chosen values are typical (4). While the efficiency and turnover time can be tuned by changing these parameters (*SI Appendix*, Fig. S1), energy-dissipating rapid short-circuiting ($\sim 10^5$/s) as in Fig. 3 *B* and *C* is never observed when the EB scheme is present. Nearly perfect one-to-one partitioning of electrons to the high- and low-potential substrates with full reversibility can be accomplished without requiring a gating mechanism (Fig. 3 *E* and *F*).

We explored the short-circuit behavior of the landscapes in Fig. 2 *G–I* as a function of the driving force ΔG_{bifurc} with this kinetic model. For the landscape of Fig. 2*I*, the electron flux away from A_L and into A_H is large ($\sim 10^6$ electrons/s), reflecting short-circuit–dominated kinetics. For landscape H, the short-circuiting flux is still large ($\sim 10^5$ electrons per second). Only when the slope of the branches follows landscape G (the EB scheme) do the electron fluxes into A_H and A_L have the same sign, reflecting electron bifurcation (confurcation)-dominated

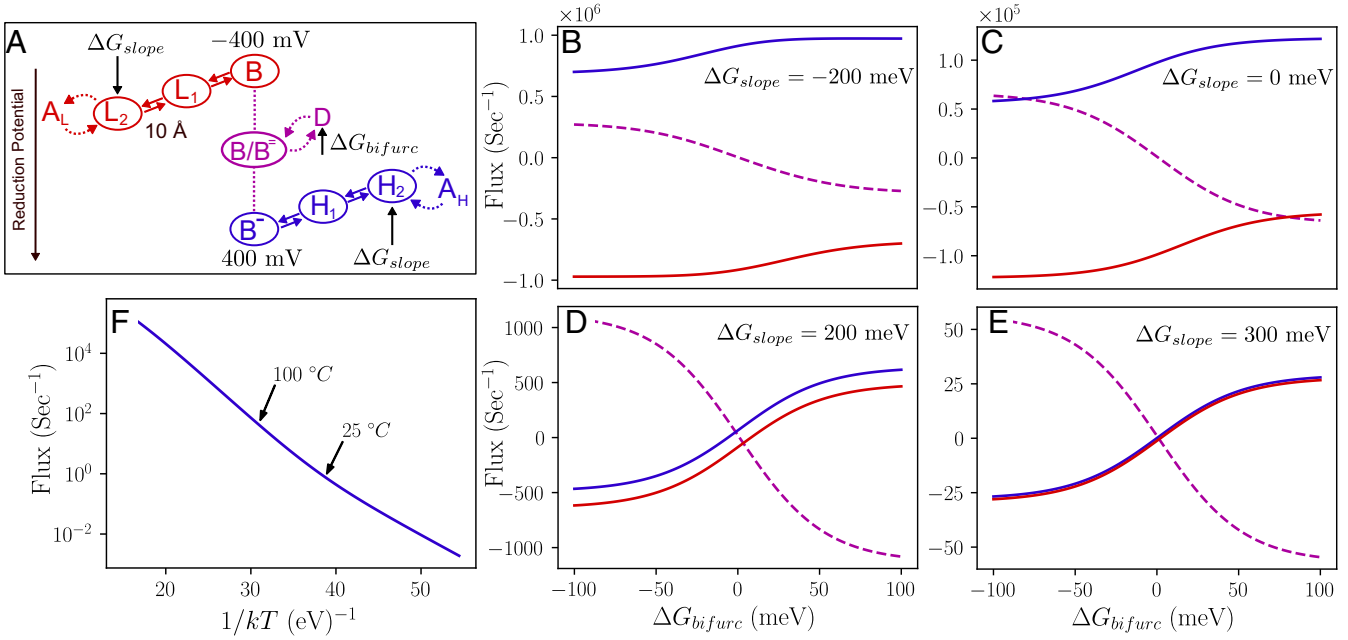

Fig. 3. Model electron bifurcation enzyme and turnover kinetics as a function of driving force. (*A*) Model electron bifurcation enzyme with cofactors spaced by 10 Å, and with the free-energy landscapes of the branches characterized by ΔG_{slope}, the energy to move an electron from the bifurcating site to the terminal substrate. The one-electron substrates were modeled as electron reservoirs with reduction potential equal to the terminal cofactor potentials on the two branches. (*B*, *C*, *E*, and *F*) Net electron fluxes into the A_H (blue), D (purple), and A_L (red) reservoirs as a function of ΔG_{bifurc}. As the slope of the branches changes from (*B*) negative, to (*C*) flat, to (*E*) positive, to (*F*) steeply positive, the dynamics change continuously from short-circuit dominated (*B* and *C*) to electron bifurcation/confurcation dominated with significant short circuits (*E*), to transduction with negligible short-circuiting (*F*). The magnitudes of all fluxes significantly drop with increasing ΔG_{slope}, reflecting the high-energy barriers for electron flux between substrates in the EB scheme. For $\Delta G_{slope} = 300$meV and $\Delta G_{bifurc} = 0$, the inverse-temperature dependence of the short-circuit fluxes (*D*) has two clear linear regimes, which indicates a thermally activated mechanism (note the log-linear plot).

kinetics when the overall driving force ΔG_{bifurc} is negative (positive). Any difference between the A_H and A_L oxidation/reduction rates (separation between the red and blue curves) reflects short-circuiting behavior, so the near-superposition of the curves in Fig. 3*F* indicates very low short-circuit currents.

The EB Scheme Suppresses Electron Short-Circuiting

When the magnitude of the energetic slopes of the two EB-scheme redox pathways is increased (Fig. 3*F*), the short-circuiting flux shrinks compared to the electron bifurcating/confurcating turnover rates, as reflected in the negligible difference between the electron fluxes into/out of the A_L and A_H reservoirs. Using the EB scheme, electron bifurcation can achieve high efficiency (equal partitioning of electrons into the A_L and A_H reservoirs), at the cost of turnover speed and reducing power of the low-potential acceptor A_L. Presumably, electron bifurcation enzymes in nature evolved to balance these tradeoffs, insulating against short circuits while enabling catalysis to proceed with sufficient speed to meet physiological demands. Importantly, alternate gating mechanisms are not required for reversible and efficient electron bifurcation in the EB scheme. In fact, electron bifurcation and confurcation emerge naturally from the kinetic network (Fig. 2*G* and 3*A*) at steady state, but only when the EB scheme is employed. Our model does not unnaturally privilege productive electron transfers over short circuits in any way. Indeed, short-circuit electron transfers are successfully insulated in the EB scheme, even when the short-circuit rate constants are set orders of magnitude faster than the productive electron transfers, due to the cofactor occupancy blockade effects (*SI Appendix*, Fig. S1*D*).

When short-circuit fluxes are small (i.e., as occurs in the EB scheme), the high- and low-potential redox branches quickly reach approximate chemical equilibrium with themselves, despite being out of equilibrium with the other branch (6) (i.e., quasi-equilibrium). Thus, the short-circuit fluxes are thermally activated. Fig. 3*D* shows the short-circuit flux into the high-potential A_H reservoir when $\Delta G_{bifurc} = 0$ (the electron bifurcation enzyme is "idling") as a function of temperature, where two distinct linear regimes are observed at low and high temperature, which indicates a thermally activated tunneling mechanism for the short circuits (this linear behavior is analyzed in detail in *SI Appendix*). The high-temperature regime is dominated by B^--mediated short circuits, which are fast but have a large thermal activation energy. The low-temperature regime is dominated by the L_1 to H_1 short circuit, which is slower but has a smaller thermal activation energy, allowing this short circuit to dominate at low temperatures.

The energetic landscapes of electron bifurcation have been proposed to be important many times before (e.g., see refs. 3–5, 28, 32, and 36.), but the special and universal nature of the EB scheme to nearly eliminate short circuits and remain fully reversible has not been shown previously. This is because a minimalistic model must include the potent combination of: 1) reversibility (20, 21), 2) explicit tracking of the entire enzyme's redox state (not just the average state of each cofactor) (35, 37), 3) three explicit electron reservoirs that are each free to exchange electrons in the branches at each reservoir's chemical potential, and 4) the explicit modeling of the energetic slopes along the entire length of the high- and low-potential branches, not just the cofactors near the bifurcating site (6). The model described here explicitly shows a reverse electron flux with negligible short-circuiting when the driving force, ΔG_{bifurc}, is reversed, unlike many previous models.

While reversibility, electron blockading, and explicit reservoirs are crucial to capture efficient electron bifurcation, combining all three into a tractable kinetic model is not simple because the number of differential equations governing the kinetics grows

exponentially with the number of cofactors (35, 37). To construct the very large model that underpins Fig. 3, we procedurally generated the equations governing the dynamics (*SI Appendix*). In fact, our model is similar to that found in refs. 35 and 37, except that we answer quantitatively the apparently central question, namely why electron bifurcation enzymes never use any of the landscapes in Fig. 2, aside from landscape G. Understanding precisely how landscape G insulates against short circuits allows us to make the strong prediction that landscape G of Fig. 2 (the EB scheme) is universal in electron bifurcation, and that this scheme is key for the design of synthetic electron bifurcation systems (see the final section below).

Interestingly, the privileged EB-scheme landscape follows a free-energy profile that is similar to the steep slopes in reduction potentials that are found in the Z scheme of photosynthesis (29), However, the mechanism of electron flow in bifurcating enzymes is drastically different, as a consequence of the reversibility of electron bifurcation reactions, in contrast to strongly driven photosynthetic reactions.

Electron bifurcation enzymes can surely exhibit complexities that are not captured in our model. For example, proton-coupled electron transfer (5, 6), two-electron cofactors (flavins or quinones) in the H and L branches (22), conformational changes (23, 39), and electron transfer between electron bifurcation monomers (40) may all add kinetic richness. In fact, conformational motion in the Q cycle is understood to be required for electrons to reach the high-potential cytochrome c_1, which is too far away for direct electron tunneling from the electron bifurcation Q_o site (33). However, none of these specific features interfere with the essential short-circuit–insulating nature of the conserved and predicted universal EB scheme.

Short-Circuiting in the Q Cycle

A fully detailed kinetic model of the Q cycle is beyond the scope of this study, but a simplified model is sufficient to account for the primary cause behind the short-circuit insulation in the Q cycle. Our model (Fig. 4*A*) uses distances and energetics suggested by experiment and indicates that the electron bifurcation energy landscape explains most of the short-circuit insulation in the Q cycle (see also *SI Appendix*, *Supplementary Text*). Cofactor reduction potentials were measured previously (28), and the tunneling distance values were used in previous studies (33). The first electron transfer from Q_o to ISP (ISP = iron–sulfur protein) is proton-coupled and rate limiting (6). This was modeled by setting an effective electron tunneling distance, which was tuned until the overall steady-state turnover was ∼50/s, placing the model in quantitative agreement with experimental steady-state turnover rates (6, 40). This fitting procedure forced the SQ → ISP (SQ = semiquinone) short-circuit rate constant to be favored over the productive HQ → ISP (HQ = hydroquinone) rate constant by several orders of magnitude. Even with this preference for a short-circuit rate constant over a productive one, short circuits were still successfully insulated (Fig. 4 *B* and *C*). The motion of the ISP was not explicitly modeled, but was assumed to

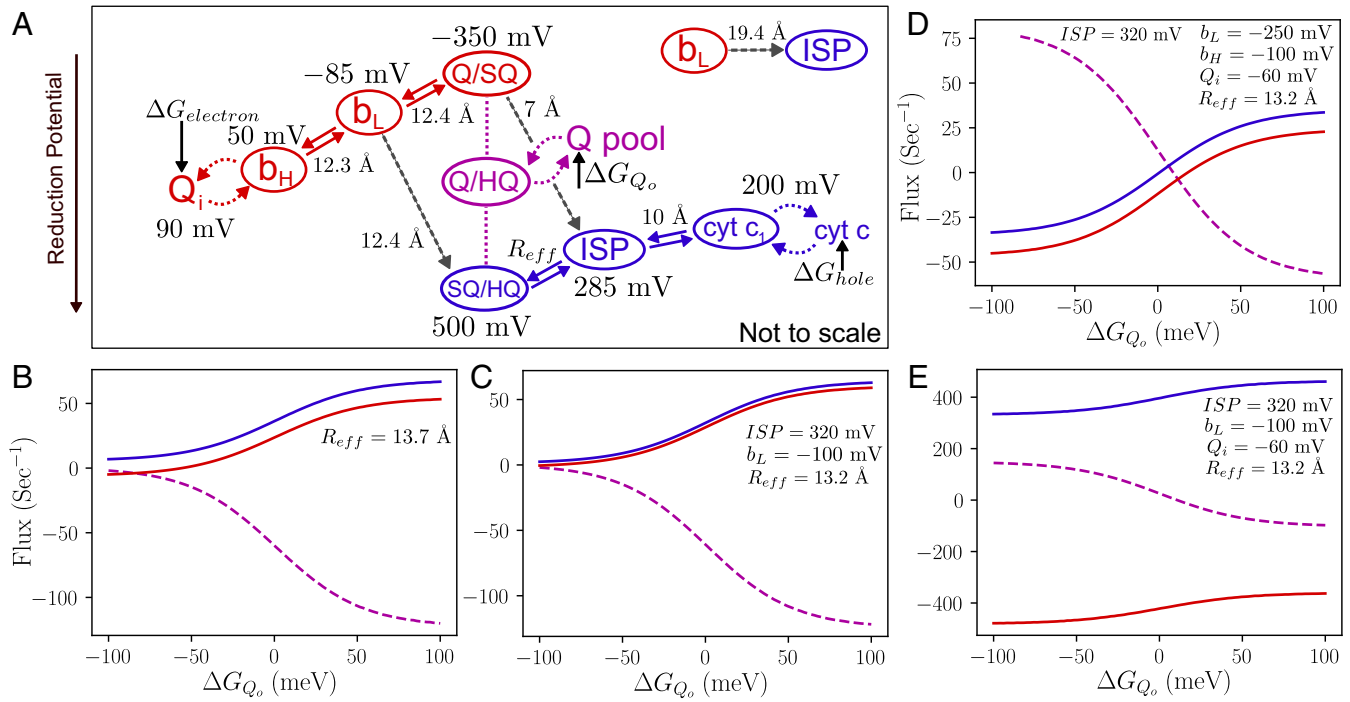

Fig. 4. Short-circuit insulation in the Q cycle (complex III) arising from the EB scheme. Using our multielectron kinetic model (*SI Appendix*), we built a simplified model (*A*) for the Q cycle using previously published reduction potentials and tunneling distances (28, 33). Despite these simplifications, the EB scheme observed in the measured reductions potentials seems (*B*) effective at insulating against short circuits. With minor changes to the reduction potentials (designed to increase $\Delta G_{electron}$ and ΔG_{hole} of the activation process shown in *SI Appendix*, Fig. S2*D*) that are likely within the range of experimental uncertainty (*C*), the EB scheme of the Q cycle provides the preponderance of insulation against short-circuiting. In *B* and *C*, no confurcation appears for the values of ΔG_{Q_o} shown since the reduction potentials cited were measured in the absence of the membrane potential (28), by which energy is ultimately conserved in the Q cycle. The influence of the membrane potential on all of the cofactor reduction potentials (and hence the EB scheme) is unknown. We present two possible cases, chosen to reflect the range of possible impacts of the membrane potential on the L-branch cofactor reduction potentials. In *D* the reduction potentials of the low-potential branch all decrease by 150 mV. In *E* the reduction potential of the Q_i site alone decreases by 150 mV. In the case of *D*, the electron bifurcation landscape may be sufficiently preserved to insulate from short circuits. In *E*, the electron bifurcation landscape is significantly disrupted, as the energy required to move an electron to cytochrome b_L (in *SI Appendix*, Eq. **S8**) in order to initiate short-circuiting is negligible. This disruption of the landscape turns on short-circuiting, but may not reflect the reality of cytochrome bc_1 in the presence of a membrane potential.

be sufficiently fast so that electrons can tunnel directly to cytochrome c_1 once ISP is reduced. The Q_i site was modeled as a one-electron reservoir, since the two one-electron reduction potentials of ubiquinone at the Q_i site are similar (41).

A few specific experiments have been interpreted as indicating a need for gating mechanisms in the Q cycle to assure its efficient function. For instance, in the Q cycle of cytochrome bc_1, the inhibitor antimycin A (which prevents electrons from leaving the low-potential branch) is known to decrease the overall steady-state turnover by a factor of about 30 (6, 40). Gating mechanisms were proposed to explain this slowdown of the redox flux with a compromised L branch (20, 21, 33, 37). Our simplified model of the Q cycle using experimental parameters (Fig. 4) shows that the EB scheme insulates against short circuits in that system. Not surprisingly, slower turnover is not observed in our simplified kinetics model with an inhibited L branch as compared to the uninhibited case (*SI Appendix*, Fig. S3), which suggests that additional features not captured in our model play a role in the Q cycle.

Molecular features behind the observed difference between uninhibited and L-branch inhibited kinetics in the Q cycle may include subtle structural changes resulting in tunneling distance changes of about 3 Å or less between the Q_o site and its iron–sulfur cofactor partner (*SI Appendix*, Fig. S3), or subtle electrostatic interactions between the low-potential branch and the Q_o site (*SI Appendix*; these are likely not the only possible explanations), rather than by a gating mechanism per se. Because the measured change in steady-state turnover in the presence of inhibitors and L-branch cofactor knockouts (20, 40) is so subtle [about a factor of 30 less (40)], these and other mechanisms will be difficult to identify uniquely (See *SI Appendix* for extended discussion).

The effect of the EB scheme in preventing short circuits is orders of magnitude larger than the observed difference between the L-branch inhibited and noninhibited turnover. Specifically, the rate constants for short-circuit electron transfers are $\sim 10^9$/s (35), which must be defeated. In the absence of additional assistance from protein gating, the EB scheme will reduce the flux to $\sim 10^2$/s, and these values will be further reduced if the L branch is not inhibited (Figs. 3 and 4), supporting the central role played by the electron bifurcation landscape in defeating short circuits. Only about one additional order of magnitude is needed to bring this turnover rate to the observed L-branch inhibited turnover rates ($\sim 10^0$/s) (40), which indicates that the efficiency gained by such a mechanism is less than 1% of the gain produced by the EB scheme (measuring efficiency with short-circuit rates). Thus, the EB scheme explains most of the short-circuit insulation in the Q cycle of cytochrome bc_1.

Natural Electron Bifurcation: Exploiting the EB Scheme

The important lesson learned is that any additional mechanisms in natural electron bifurcation enzymes, beyond the EB scheme, are not the key features that underpin the short-circuit insulation in electron bifurcation systems, including the Q cycle. There is a tremendous difference between a gating mechanism that changes a rate constant by nine orders of magnitude (which is required to insulate against short circuits without the EB scheme) and a mechanism that intrinsically prevents that kinetic pathway from ever being accessed by the system under normal operating conditions (this is how the EB scheme works; see *SI Appendix*, Fig. S2). Other subtle features and mechanisms might shave off the last order of magnitude or two of short-circuiting flux when the L branch is inhibited, or even permit some short-circuiting and serve as "release valves" that can reroute electrons to add robustness to biochemical pathways. For instance, certain photosynthetic bacteria were found to be able to grow with an inhibited Q cycle (42). These organisms required a short-circuit flux across a Q cycle to grow. Importantly, our analysis does not disentangle subtle features of electron bifurcation enzymes, which likely differ from system to system. We do, however, propose that the EB scheme is sufficient to accomplish robust electron bifurcation, explains the lion's share of short-circuit insulation in known electron bifurcating systems, and may serve as a core design framework for synthetic electron bifurcation systems.

Synthetic Electron Bifurcation: Exploiting the EB Scheme

The EB scheme enables reversible electron bifurcation, insulates against wasteful short-circuit reactions, and thus appears to remove the two primary roadblocks that prevent the design and synthesis of electron bifurcation molecular machines (5). A robust and general scheme to prevent short circuits suggests that synthetic electron bifurcation is not a distant dream.

We envision that the EB scheme (Fig. 2*G*) may be realized with several kinds of molecular architectures. For instance, covalently linked molecular redox species, DNA origami motifs (43), tailored linked quantum dots (44), or even semiconductor nanostructures may serve as possible frameworks in which to realize electron bifurcation. For example, the EB-scheme landscape is found in the band bending of n-p semiconductor junctions (45), which suggests that semiconductors may play a role in synthetic electron bifurcation.

In the EB scheme, each redox site other than the bifurcating site must be made to accommodate only one mobile electron at a time and must not be allowed to interact further than its nearest neighbors. For example, if L_2 could donate an electron to H_2 (Fig. 1), or if H_1 could receive several electrons from $B^=$, the EB scheme would no longer insulate against short circuits (these processes were included in our model, but since the distance between nonneighbor cofactors is at least 20 Å in the model, the corresponding tunneling rate constant is negligibly small). In addition, the terminal electron acceptors, D, A_L, and A_H, must not exchange electrons directly with each other, or with any of the redox active sites in the scaffold, other than with the terminal branch sites. This level of microscopic control is challenging to realize, and anchoring the A_L and A_H acceptors to the ends of the branches may be acceptable for proof-of-concept experiments. Care must also be taken to avoid short-circuit channels during the $D^=$ to B electron refilling process (short-circuiting during refilling).

Electron bifurcation in nature allows the reversible reduction of compounds with low reduction potentials, using compounds with much higher (midpoint) reduction potentials, analogous to the function of a voltage amplifier. Understanding the manner of this redox conversion in the warm, wet environment of biology provides inspiration for novel synthetic redox catalysts.

Data Availability

Python data have been deposited in GitHub (https://github.com/JYuly/EB_kinetics). All other study data are included in the article and *SI Appendix*.

ACKNOWLEDGMENTS. This work is supported as part of the Biological Electron Transfer and Catalysis EFRC, an Energy Frontier Research Center funded by a grant from the US Department of Energy, Office of Science (DE-SC0012518). This work was authored in part by Alliance for Sustainable Energy, LLC, the manager and operator of the National Renewable Energy Laboratory for the US Department of Energy (DOE) under Contract DE-AC36-08GO28308. Funding was provided to C.E.L. by the US DOE Office of Basic Energy Sciences, Division of Chemical Sciences, Geosciences, and Biosciences, Physical Biosciences Program. The US Government and the publisher, by accepting the article for publication, acknowledges that the US Government retains a nonexclusive, paid-up, irrevocable, worldwide license to publish or reproduce the published form of this work, or allow others to do so, for US Government purposes. We thank Gerrit Schut for helpful discussions.

1. P. Mitchell, The protonmotive Q cycle: A general formulation. *FEBS Lett.* **59**, 137–139 (1975).
2. J. W. Peters, A.-F. Miller, A. K. Jones, P. W. King, M. W. Adams, Electron bifurcation. *Curr. Opin. Chem. Biol.* **31**, 146–152 (2016).
3. P. Zhang *et al*., Electron bifurcation: Thermodynamics and kinetics of two-electron brokering in biological redox chemistry. *Acc. Chem. Res.* **50**, 2410–2417 (2017).
4. W. Buckel, R. K. Thauer, Flavin-based electron bifurcation, a new mechanism of biological energy coupling. *Chem. Rev.* **118**, 3862–3886 (2018).
5. J. L. Yuly, C. E. Lubner, P. Zhang, D. N. Beratan, J. W. Peters, Electron bifurcation: Progress and grand challenges. *Chem. Commun.* **55**, 11823–11832 (2019).
6. A. R. Crofts *et al*., The mechanism of ubihydroquinone oxidation at the Q_o-site of the cytochrome bc_1 complex. *Biochim. Biophys. Acta* **1827**, 1362–1377 (2013).
7. C. N. Hunter, F. Daldal, M. C. Thurnauer, J. T. Beatty, Eds., *The Purple Phototrophic Bacteria*, (Springer Science & Business Media, 2008), Vol. 28.
8. A. K. Kaster, J. Moll, K. Parey, R. K. Thauer, Coupling of ferredoxin and heterodisulfide reduction via electron bifurcation in hydrogenotrophic methanogenic archaea. *Proc. Natl. Acad. Sci. U.S.A.* **108**, 2981–2986 (2011).
9. T. Wagner, J. Koch, U. Ermler, S. Shima, Methanogenic heterodisulfide reductase (HdrABC-MvhAGD) uses two noncubane [4Fe-4S] clusters for reduction. *Science* **357**, 699–703 (2017).
10. R. N. Ledbetter *et al*., The electron bifurcating FixABCX protein complex from *Avotobacter vinlandii*: Generation of low-potential reducing equivalents for nitrogenase catalysis. *Biochemistry* **56**, 4177–4190 (2017).
11. G. J. Schut, M. W. W. Adams, The iron-hydrogenase of Thermotoga maritima utilizes ferredoxin and NADH synergistically: A new perspective on anaerobic hydrogen production. *J. Bacteriol.* **191**, 4451–4457 (2009).
12. W. Buckel, R. K. Thauer, Flavin-based electron bifurcation, ferredoxin, flavodoxin, and anaerobic respiration with protons (Ech) or NAD^+ (Rnf) as electron acceptors: A historical review. *Front. Microbiol.* **9**, 401 (2018).
13. V. Müller, N. P. Chowdhury, M. Basen, Electron bifurcation: A long-hidden energy-coupling mechanism. *Annu. Rev. Microbiol.* **72**, 331–353 (2018).
14. F. Baymann *et al*., On the natural history of flavin-based electron bifurcation. *Front. Microbiol.* **9**, 1357 (2018).
15. W. Buckel, R. K. Thauer, Energy conservation via electron bifurcating ferredoxin reduction and proton/$Na(^+)$ translocating ferredoxin oxidation. *Biochim. Biophys. Acta* **1827**, 94–113 (2013).
16. N. P. Chowdhury *et al*., Studies on the mechanism of electron bifurcation catalyzed by electron transferring flavoprotein (Etf) and butyryl-CoA dehydrogenase (Bcd) of *Acidaminococcus fermentans*. *J. Biol. Chem.* **289**, 5145–5157 (2014).
17. R. K. Thauer, My lifelong passion for biochemistry and anaerobic microorganisms. *Annu. Rev. Microbiol.* **69**, 1–30 (2015).
18. J. W. Peters *et al*., A new era for electron bifurcation. *Curr. Opin. Chem. Biol.* **47**, 32–38 (2018).
19. J. W. Peters, D. N. Beratan, G. J. Schut, M. W. W. Adams, On the nature of organic and inorganic centers that bifurcate electrons, coupling exergonic and endergonic oxidation-reduction reactions. *Chem. Commun.* **54**, 4091–4099 (2018).
20. A. Osyczka, C. C. Moser, F. Daldal, P. L. Dutton, Reversible redox energy coupling in electron transfer chains. *Nature* **427**, 607–612 (2004).
21. A. Osyczka, C. C. Moser, P. L. Dutton, Fixing the Q cycle. *Trends Biochem. Sci.* **30**, 176–182 (2005).
22. C. E. Lubner *et al*., Mechanistic insights into energy conservation by flavin-based electron bifurcation. *Nat. Chem. Biol.* **13**, 655–659 (2017).
23. E. A. Berry, L.-S. Huang, Conformationally linked interaction in the cytochrome $bc_{(1)}$ complex between inhibitors of the $Q_{(o)}$ site and the Rieske iron-sulfur protein. *Biochim. Biophys. Acta* **1807**, 1349–1363 (2011).
24. A. R. Crofts *et al*., The Q-cycle mechanism of the bc_1 complex: A biologist's perspective on atomistic studies. *J. Phys. Chem. B* **121**, 3701–3717 (2017).
25. A. R. Crofts, S. Lhee, S. B. Crofts, J. Cheng, S. Rose, Proton pumping in the bc_1 complex: A new gating mechanism that prevents short circuits. *Biochim. Biophys. Acta* **1757**, 1019–1034 (2006).
26. R. K. Thauer, A.-K. Kaster, H. Seedorf, W. Buckel, R. Hedderich, Methanogenic archaea: Ecologically relevant differences in energy conservation. *Nat. Rev. Microbiol.* **6**, 579–591 (2008).
27. J. K. Demmer, N. Pal Chowdhury, T. Selmer, U. Ermler, W. Buckel, The semiquinone swing in the bifurcating electron transferring flavoprotein/butyryl-CoA dehydrogenase complex from Clostridium difficile. *Nat. Commun.* **8**, 1577 (2017).
28. L. Bergdoll, F. Ten Brink, W. Nitschke, D. Picot, F. Baymann, From low- to high-potential bioenergetic chains: Thermodynamic constraints of Q-cycle function. *Biochim. Biophys. Acta* **1857**, 1569–1579 (2016).
29. R. E. Blankenship, *Molecular Mechanisms of Photosynthesis*, (John Wiley & Sons, ed. 2, 2014).
30. J. Blumberger, Recent advances in the theory and molecular simulation of biological electron transfer reactions. *Chem. Rev.* **115**, 11191–11238 (2015).
31. D. N. Beratan, J. N. Onuchic, J. R. Winkler, H. B. Gray, Electron-tunneling pathways in proteins. *Science* **258**, 1740–1741 (1992).
32. W. Nitschke, M. J. Russell, Redox bifurcations: Mechanisms and importance to life now, and at its origin. *BioEssays* **34**, 106–109 (2012).
33. C. C. Moser, T. A. Farid, S. E. Chobot, P. L. Dutton, Electron tunneling chains of mitochondria. *Biochim. Biophys. Acta* **1757**, 1096–1109 (2006).
34. C. L. Quinlan, A. A. Gerencser, J. R. Treberg, M. D. Brand, The mechanism of superoxide production by the antimycin-inhibited mitochondrial Q-cycle. *J. Biol. Chem.* **286**, 31361–31372 (2011).
35. S. Ransac, N. Parisey, J.-P. Mazat, The loneliness of the electrons in the bc_1 complex. *Biochim. Biophys. Acta* **1777**, 1053–1059 (2008).
36. D. Victoria, R. Burton, A. R. Crofts, Role of the -PEWY-glutamate in catalysis at the Q_o-site of the Cyt bc_1 complex. *Biochim. Biophys. Acta* **1827**, 365–386 (2013).
37. S. Ransac, J.-P. Mazat, How does antimycin inhibit the bc_1 complex? A part-time twin. *Biochim. Biophys. Acta* **1797**, 1849–1857 (2010).
38. R. A. Marcus, N. Sutin, Electron transfers in chemistry and biology. *Biochim. Biophys. Acta* **811**, 265–322 (1985).
39. D. Xia *et al*., Crystal structure of the cytochrome bc_1 complex from bovine heart mitochondria. *Science* **277**, 60–66 (1997).
40. M. Świerczek *et al*., An electronic bus bar lies in the core of cytochrome bc_1. *Science* **329**, 451–454 (2010).
41. H. Zhang *et al*., Quinone and non-quinone redox couples in Complex III. *J. Bioenerg. Biomembr.* **40**, 493–499 (2008).
42. A. Malnoë, F.-A. Wollman, C. de Vitry, F. Rappaport, Photosynthetic growth despite a broken Q-cycle. *Nat. Commun.* **2**, 301 (2011).
43. N. V. Voigt *et al*., Single-molecule chemical reactions on DNA origami. *Nat. Nanotechnol.* **5**, 200–203 (2010).
44. B. P. Bloom *et al*., Directing charge transfer in quantum dot assemblies. *Acc. Chem. Res.* **51**, 2565–2573 (2018).
45. N. W. Ashcroft, N. D. Mermin, *Solid State Physics*, (Holt, Rinehart, and Winston, 1976).